OPEN

Diagnostic Value of ^{18}F-FACBC PET/MRI in Brain Metastases

Silje Kjærnes Øen, PhD,† Knut Johannessen,* Lars Kjelsberg Pedersen, MD,‡ Erik Magnus Berntsen, MD, PhD,*† Jon Andre Totland, MD,§ Håkon Johansen, MD,† Trond Velde Bogsrud, MD, PhD,||¶ Tora S. Solheim, MD, PhD,**†† Anna Karlberg, PhD,*† and Live Eikenes, PhD*†*

Purpose: The study aims to evaluate whether combined ^{18}F-FACBC PET/MRI could provide additional diagnostic information compared with MRI alone in brain metastases.

Patients and Methods: Eighteen patients with newly diagnosed or suspected recurrence of brain metastases received dynamic ^{18}F-FACBC PET/MRI. Lesion detection was evaluated on PET and MRI scans in 2 groups depending on prior stereotactic radiosurgery (SRS group) or not (no-SRS group). SUVs, time-activity curves, and volumetric analyses of the lesions were performed.

Results: In the no-SRS group, 29/29 brain lesions were defined as "MRI positive." With PET, 19/29 lesions were detected and had high tumor-to-background ratios (TBRs) ($D_{max\ MR}$, ≥7 mm; SUV_{max}, 1.2–8.4; TBR, 3.9–25.9), whereas 10/29 lesions were undetected ($D_{max\ MR}$, ≤8 mm; SUV_{max}, 0.3–1.2; TBR, 1.0–2.7). In the SRS group, 4/6 lesions were defined as "MRI positive," whereas 2/6 lesions were defined as "MRI negative" indicative of radiation necrosis. All 6 lesions were detected with PET ($D_{max\ MR}$, ≥15 mm; SUV_{max}, 1.4–4.2; TBR, 3.6–12.6). PET volumes correlated and were comparable in size with contrast-enhanced MRI volumes but were only partially congruent (mean DSC, 0.66). All time-activity curves had an early peak, followed by a plateau or a decreasing slope.

Conclusions: ^{18}F-FACBC PET demonstrated uptake in brain metastases from cancer of different origins (lung, gastrointestinal tract, breast, thyroid, and malignant melanoma). However, ^{18}F-FACBC PET/MRI did not improve detection of brain metastases compared with MRI but might detect tumor tissue beyond contrast enhancement on MRI. ^{18}F-FACBC PET should be further evaluated in recurrent brain metastases.

Key Words: brain metastases, ^{18}F-FACBC, PET, contrast enhancement, MRI, detection

(*Clin Nucl Med* 2022;47: 1030–1039)

Received for publication May 30, 2022; revision accepted September 8, 2022.

From the *Department of Circulation and Medical Imaging, Faculty of Medicine and Health Sciences, Norwegian University of Science and Technology; †Department of Radiology and Nuclear Medicine, St. Olavs Hospital, Trondheim University Hospital, Trondheim; ‡Department of Neurosurgery, §Department of Radiology, and ||PET Centre, University Hospital of North Norway, Tromsø, Norway; ¶PET Centre, Aarhus University Hospital, Aarhus, Denmark; **Cancer Clinic, St. Olavs Hospital, Trondheim University Hospital; and ††Department of Clinical and Molecular Medicine, Norwegian University of Science and Technology, Trondheim, Norway.

Conflicts of interest and sources of funding: The authors declare that they have no conflicts of interest. The work was supported by Trond Mohn Foundation.

Correspondence to: Silje Kjærnes Øen, PhD, Department of Circulation and Medical Imaging, Faculty of Medicine and Health Sciences, Norwegian University of Science and Technology, Post Box 8905, N-7491 Trondheim, Norway. E-mail: silje.kjernes.oen@stolav.no.

ISSN: 0363-9762/22/4712–1030
DOI: 10.1097/RLU.0000000000004435

It is estimated that 10% to 40% of patients with cancer will develop 1 or more brain metastases.[1–3] These originate most frequently from lung cancer, followed by breast cancer and malignant melanoma.[4] Patients with brain metastases have a poor prognosis with a median survival of 6 months and a 2-year survival of 8.1%.[5,6] Stereotactic radiosurgery (SRS) is frequently the preferred treatment for patients with brain metastases, but whole-brain radiation therapy, neurosurgical resection, and/or systemic treatments such as chemotherapy, immunotherapies, and targeted therapy can also be considered.[7,8] Late diagnosis may limit treatment options,[9] and early identification and accurate localization of brain metastases are therefore important for treatment planning and preventing further deterioration of the patient.[10] Precise tumor delineation and tools to differentiate brain metastases from treatment-related changes, such as radiation necrosis, are also of high importance.

Contrast-enhanced MRI (ce-MRI) is currently the recommended imaging modality for the detection of brain metastases.[11] MRI provides high-resolution anatomical images with excellent soft tissue contrast, and contrast agents increase visibility of pathology when the blood-brain barrier (BBB) is disrupted. Brain metastases are considered to be well delineated on ce-MRI, and the sensitivity for detection is high also for small metastases. However, contrast enhancement is a marker for BBB disruption, which may be caused by radiotherapy, infection, inflammation, ischemia, and other afflictions.[11] Contrast enhancement is therefore not specific for malignancy, and ce-MRI has limitations for instance in separating recurrence of brain metastases from treatment-related changes, a challenge regularly occurring in clinical practice. The accuracy may be improved with perfusion-weighted MRI, but the literature is still limited, and alternative tools for diagnosing recurrent brain metastases after treatment are warranted.[12]

Amino acid (AA) PET may add complementary information to MRI in the management of patients with brain metastases. Brain malignancies accumulate AAs through overexpression of AA transporter systems, which is a result of alterations in tumor vasculature and proliferation.[13] Amino acid PET tracers do not accumulate as much in normal brain parenchyma as the most commonly used PET tracer, the glucose analog ^{18}F-FDG. This results in improved tumor-to-normal brain contrast for AA tracers over ^{18}F-FDG. The transport of AAs across the BBB is facilitated by specific AA transporters, which allows for uptake in neoplastic tissue even with an intact BBB for common AA tracers, in contrast to MRI.[14]

Amino acid PET tracers (i.e., ^{11}C-methyl-L-methionine [^{11}C-MET], *O*-[2-^{18}F-Fluoroethyl]-L-tyrosine [^{18}F-FET], and L-3,4-dihydroxy-6-^{18}F-fluorophenylalanine [^{18}F-FDOPA]) are recommended by international guidelines to complement MRI in the clinical management of patients with gliomas.[13,15,16] For patients with brain metastases, the Response Assessment in Neuro-Oncology (RANO) working group has concluded that ce-MRI is the imaging modality of choice for detecting brain metastases due to the high spatial resolution.[11] However, the RANO group has also stated that AA PET is useful for differentiating brain metastasis recurrence from radiation-induced changes, but

that the literature is still limited.[11] ^{18}F-FET has shown to differentiate recurrence of brain metastases from radiation necrosis with high accuracy, especially when supplemented with dynamic PET acquisitions.[17–19]

The artificial AA anti-1-amino-3-^{18}F-fluorocyclobutane-1-carboxylic acid (^{18}F-FACBC),[20] also known as fluciclovine (^{18}F) or Axumin (Blue Earth Diagnostics Ltd, United Kingdom), was initially developed for the assessment of brain tumors but is most commonly used for prostate cancer.[21] Recent studies have demonstrated increased ^{18}F-FACBC uptake in gliomas compared with normal brain parenchyma, especially for high-grade gliomas.[22–28] Several glioma studies have reported ^{18}F-FACBC uptake in areas without contrast enhancement, in addition to generally larger tumor volumes with ^{18}F-FACBC than ce-MRI.[22,24,27,29] In addition, in studies exploring glioma, ^{18}F-FACBC provides greater visual contrast than ^{11}C-MET due to lower uptake in healthy brain tissue.[25,26,29] This high contrast has likely also allowed for the detection of small satellite gliomas not visualized with MRI.[23]

^{18}F-FACBC PET has only been evaluated in a limited number of patients with brain metastases.[30,31] The results are promising with relatively high tumor-to-background ratios (TBRs) compared with ^{18}F-FET and ^{11}C-MET. This may increase the possibility to detect small brain metastases. ^{18}F-FACBC PET has also shown potential to differentiate recurrence from radiation necrosis.[30] The potential of ^{18}F-FACBC in the management of brain metastases should therefore be further explored. The aims of this study were to assess the diagnostic value of static and dynamic ^{18}F-FACBC PET in patients with brain metastases and to compare tumor volumes between ^{18}F-FACBC PET and ce-MRI.

PATIENTS AND METHODS

Subjects

Between January 2020 and July 2021, 18 patients (7 female) were recruited to a multicenter study at St. Olavs Hospital, Trondheim University Hospital, and the University Hospital of Northern Norway for simultaneous brain ^{18}F-FACBC PET/MRI examinations. Patients were eligible for inclusion if they had a known or confirmed cancer and MRI findings consistent with a new metastatic brain lesion and/or suspected recurrence if previously treated with surgery or SRS in this location.

The average age of the subjects was 64.5 years (range, 51–77 years), and their primary cancers were lung (n = 9), gastrointestinal (GI) (n = 5), malignant melanoma (n = 2), breast (n = 1), and thyroid (n = 1) (Tables 1 and 2). The patients had a median graded prognostic assessment of 1.5 (range, 0–3).[32] Four patients (4 lesions) had prior intracerebral resection, and 4 patients (6 lesions) had prior SRS in the same location as the lesion of interest. One patient received chemotherapy (FOLFOX + SOX), and 1 patient had immunotherapy treatment (nivolumab, Opdivo; Bristol-Myers Squibb) during the last month before the PET/MRI examination. Thirteen patients had ongoing glucocorticosteroid treatment at the time of the examination. The study was approved by the Regional Ethics Committee (REC, reference number: 2018/2243). All patients gave written informed consent to participate in the study.

PET/MRI

The patients underwent a simultaneous brain PET/MRI examination (Siemens Biograph mMR; Erlangen, Germany) after at least 4 hours of fasting. ^{18}F-FACBC (3.0 ± 0.2 MBq/kg; average activity, 234 ± 50 MBq) was manually injected at $t = 0$ of the PET acquisition (list mode; 0–35 minutes post injection). Two patients (ID 10 and 11) had a shorter acquisition (30 minutes) due to delays and expiration of the tracer. MRI sequences acquired were ultrashort echo time (UTE) for PET attenuation correction, 3D fluid-attenuated inversion recovery, and contrast-enhanced 3D T1 magnetization-prepared rapid gradient echo. One patient (ID 12) was examined on a PET/CT system (Siemens Biograph Vision 600) due to technical problems with the PET/MRI system (only static acquisition 20–35 minutes post injection). This patient had a separate MRI examination later the same day.

PET Reconstruction

Static and dynamic PET image reconstructions were performed using iterative OSEM reconstruction (PET/MRI reconstruction: 3 iterations, 21 subsets, 344 image matrix, 4 mm Gaussian filter; PET/CT reconstruction: 8 iterations, 5 subsets, 440 image matrix, 4 mm Gaussian filter, TOF), point spread function modeling, and relative scatter correction. MR-based attenuation correction was performed with a deep learning–based method (DeepUTE) using the UTE MR sequence as input for making MR-based attenuation correction maps.[33] Static PET reconstructions were generated from the last 15 minutes of the list mode data, whereas the dynamic reconstructions were performed with frames of 12 × 5 seconds, 6 × 10 seconds, 6 × 30 seconds, 5 × 60 seconds, and 5 × 300 seconds, based on recommendations for dynamic ^{18}F-FET PET imaging of gliomas.[16]

Image Evaluation

The PET and MR images were jointly investigated by an experienced nuclear medicine physician (years of experience: H.J., 5 years/T.V.B., 20 years) and an experienced neuroradiologist (years of experience: E.M.B., 7 years/J.A.T., 8 years). As both recurrence and radiation necrosis show contrast enhancement, the MRI interpretation differed depending on whether the lesions were treated with SRS before PET/MRI or not, and the lesions were divided in 2 groups. Lesions without previous SRS in the same location (no-SRS group) were categorized as "MRI positive" if they showed contrast enhancement and were not present on previous MRIs or if no previous MRIs were available, thus radiologically evident a metastasis. Contrast-enhancing lesions in operation cavities were also defined as "MRI positive." Lesions with previous SRS in the same location (SRS group) were categorized as "MRI positive" if showing contrast enhancement and progressive enlargement according to the RANO criteria for brain metastasis[34] (>20% enlargement in longest diameter) compared with previous MRI scans. On the contrary, if the lesions had been stable or decreased in size compared with previous MRI scans and thus indicative of radiation necrosis, they were categorized as "MRI negative." A follow-up status of the lesions in the SRS group was assessed based on follow-up MRIs after the PET/MRI, to serve as a surrogate marker for separating true recurrence from radiation necrosis in the lack of histopathological verification. PET findings with ^{18}F-FACBC uptake distinctly higher than surrounding tissue were defined as detected on PET.

Image Analysis

Image analysis was performed with the software PMOD (version 4.203; PMOD Technologies LLC, Zürich, Switzerland). A volume of interest (VOI) was drawn on the static PET images to encompass the lesion of interest to extract the SUV_{max} of the lesion. For lesions not detected on PET, SUV_{max} was measured in the volume defined on ce-MRI. To measure reference tissue, a crescent-shaped VOI was placed in normal brain parenchyma (in the contralateral hemisphere if only 1 lesion and in an area not affected by the disease if lesions in both hemispheres) as described by Unterrainer et al[35] (Fig. 1). The SUV_{mean} in the normal brain VOI was measured. TBR was defined for all brain lesions of interest in the static PET images as SUV_{max} divided by SUV_{mean}. SUV_{max} and TBR were compared between lesions of different tumor origins.

PET and MRI tumor volumes, V_{PET} and V_{MRI}, were defined subsequent to rigid registration of the static PET image to the T1 MR image to ensure best possible alignment and equal voxel dimensions. No guidelines exist for tumor delineation with ^{18}F-FACBC PET. A

TABLE 1. Patient Information and Results From Evaluations of Brain Lesions Not Treated With Stereotactic Radiosurgery (No-SRS Group) Before PET/MRI

Patient ID	Age	Primary Cancer	GPA	Lesion Number	MRI Positive*	PET Detected†	$D_{max\ MR}$, (mm)	V_{MRI}, (mL)	V_{PET}, (mL)	DSC	SUV_{max}	SUV_{mean}	TBR	TAC Slope
1‡	54	Breast	2.5	1	Yes	Yes	19	1.68	1.7	0.76	3.2	0.3	12.3	III
2	61	Esophagus (GI)	0	1§	Yes	Yes	55	5.00	9.3	0.55	3.9	0.4	9.0	III
				2	Yes	No	5	0.03	—	—	1.0	0.4	2.2	—
				3	Yes	No	5	0.02	—	—	1.2	0.4	2.7	—
				4	Yes	No	5	0.02	—	—	0.5	0.4	1.2	—
				5	Yes	No	4	0.02	—	—	0.7	0.4	1.6	—
3‡‖	63	Coli (GI)	1	1	Yes	Yes	22	2.60	2.1	0.77	7.3	0.6	12.8	III
4	66	Lung	1.5	1	Yes	Yes	10	0.32	1.0	0.50	1.8	0.3	5.4	—
5‡	66	Lung	0	1	Yes	Yes	18	1.53	2.2	0.69	3.5	0.4	8.6	III
				2	Yes	Yes	9	0.14	0.6	0.35	1.9	0.4	4.7	—
				3	Yes	No	4	0.01	—	—	0.5	0.4	1.3	—
				4	Yes	No	5	0.01	—	—	0.5	0.4	1.2	—
6‡	74	Melanoma	3	1	Yes	Yes	30	5.38	3.7	0.77	7.4	0.3	21.9	III
				2	Yes	Yes	17	0.91	0.9	0.63	3.6	0.3	10.8	III
8¶	73	Melanoma	3	1§	Yes	Yes	13	0.36	0.5	0.58	6.9	0.3	19.8	II
				2	Yes	Yes	7	0.10	0.5	0.30	1.7	0.3	4.7	—
				3	Yes	No	3	0.01	—	—	0.4	0.3	1.0	—
9‡	51	Coli (GI)	0	1	Yes	Yes	24	4.18	6.6	0.76	2.3	0.4	5.8	II
12‡	56	Esophagus (GI)	0	1	Yes	Yes	49	27.02	29.6	0.90	5.2	0.4	13.2	—
13‡	69	Thyroid	NA	1	Yes	Yes	8	0.14	0.9	0.24	1.2	0.3	3.9	—
				2	Yes	No	6	0.04	—	—	0.4	0.3	1.3	—
				3	Yes	No	5	0.02	—	—	0.3	0.3	1.1	—
				4	Yes	No	8	0.09	—	—	0.7	0.3	2.2	—
14‡	58	Lung	3	1	Yes	Yes	26	4.47	3.6	0.86	8.4	0.3	25.9	III
15‡	67	Rectal (GI)	0	1	Yes	Yes	33	7.83	10.7	0.83	3.8	0.4	10.6	II
16	74	Lung#	1.5	1	Yes	Yes	51	25.60	30.9	0.88	4.3	0.3	16.4	II
17‡	63	Lung#	0.5	1	Yes	Yes	38	12.85	10.8	0.76	6.5	0.3	21.7	III
				2	Yes	Yes	47	18.85	18.8	0.89	3.2	0.3	10.7	II
18‡	63	Lung#	3	1	Yes	Yes	38	11.30	11.7	0.78	2.8	0.3	9.2	II

*"Yes" if new contrast-enhancing lesion.

†"Yes" if visually detected on PET, "no" otherwise.

‡Ongoing steroid treatment.

§Prior resection at same location.

‖Chemotherapy last month.

¶Immunotherapy last month.

#Most likely lung cancer.

$D_{max\ MR}$, maximum lesion diameter on ce-MRI; V_{MRI}, tumor volume defined on ce-MRI; V_{PET}, tumor volume defined on ^{18}F-FACBC PET; NA, not available, GPA not defined for thyroid cancer.

threshold-based method of 41% of SUV_{max} was found to visually perform best for all lesion sizes and was applied in this study. Manual modifications were made to include necrotic areas inside tumors and to exclude nontumor tissue, such as veins. Contrast-enhanced MRI volumes were manually delineated in accordance with an experienced neuroradiologist, and necrotic areas inside tumors were included. The maximum diameter of the lesions (in any direction) on ce-MRI ($D_{max\ MR}$) was automatically calculated in PMOD. The spatial similarity of PET and MRI tumor volumes was evaluated using the Dice similarity coefficient (DSC).[36]

$$DSC = \frac{2\,(V_{MRI} \cap V_{PET})}{V_{MRI} + V_{PET}}$$

The VOIs drawn on static PET were transferred to the dynamic PET images to generate time-activity curves (TACs) for SUV_{max} and SUV_{mean}. The SUV_{max} curve was assigned to one of the following slope characteristics, as defined by Galldiks et al[17]: (I) constantly increasing uptake without identifiable peak, (II) uptake peaking early (<20 minutes) followed by a plateau, and (III) uptake peaking early (<20 minutes) followed by a constant decrease. Only PET detected lesions with $D_{max\ MR}$ >10 mm were included in the dynamic analyses, due to generally poor activity recovery for small lesions.[37]

Statistics

Statistical analyses were performed with MATLAB (R2021a, The MathWorks). The Wilcoxon rank sum test was used to test

TABLE 2. Patient Information and Results From Evaluations of Brain Lesions Treated With Stereotactic Radiosurgery (SRS Group) Before PET/MRI

Patient ID	Age	Primary Cancer	GPA	Lesion Number	Time Since SRS	MRI Positive*	PET Detected†	Follow-up Status‡ (TP After PET/MRI)	$D_{max\ MR}$ (mm)	V_{MRI} (mL)	V_{PET} (mL)	DSC	SUV_{max}	SUV_{mean}	TBR	TAC Slope
7	60	Lung	1.5	1§‖	1 y	No	Yes	Lesion stable, but 7 new brain lesions (10 mo)	36	3.2	4.4	0.57	4.1	0.4	10.6	II
9¶	51	Coli (GI)	0	2§‖		Yes	Yes	Deceased (5 mo)	20	1.6	2.2	0.59	3.0	0.4	7.6	III
				3§	6 mo	Yes	Yes		15	0.8	2.4	0.52	1.4	0.4	3.6	II
				4§		Yes	Yes		31	6.5	10.1	0.76	2.5	0.4	6.5	II
10¶	66	Lung	2	1§	2.5 y	Yes	Yes	Deceased (5 mo)	34	5.9	6.5	0.80	4.2	0.3	12.6	II
11¶	77	Lung	1	1§	1 y	No	Yes	Lesion stable (7 mo)	23	1.7	3.0	0.58	3.8	0.4	9.3	II

*"Yes" if lesion showed contrast enhancement and progressive enlargement compared with previous MRIs, "no" if lesion was stable or decreased in size compared with previous MRIs.

†"Yes" if visually detected on PET.

‡Based on follow-up MRI.

§Prior SRS at same location.

‖Prior resection at same location.

¶Ongoing steroid treatment.

GPA, graded prognostic assessment; TP, time period, $D_{max\ MR}$, maximum lesion diameter on ce-MRI; V_{MRI}, tumor volume defined on ce-MRI; V_{PET}, tumor volume defined on ^{18}F-FACBC PET.

differences in PET and MRI volumes, whereas Spearman ρ, r_s, was calculated to evaluate the correlation between the volumes.

RESULTS

Static PET Versus MRI

The results in the no-SRS group are presented in Table 1. Twenty-nine lesions were identified with MRI in the no-SRS group, and all lesions were defined as "MRI positive." Nineteen of 29 lesions were detected with ^{18}F-FACBC PET and had in general high ^{18}F-FACBC uptake and TBR (SUV_{max}: mean, 4.2 ± 2.2; range, 1.2–8.4; TBR: mean, 12.0 ± 6.5; range, 3.9–25.9). All PET detected lesions had $D_{max\ MR}$ ≥7 mm. Ten of 29 lesions were undetected with ^{18}F-FACBC PET due to low ^{18}F-FACBC uptake and TBR (SUV_{max}: mean, 0.6 ± 0.3; range, 0.3–1.2; TBR: mean, 1.6 ± 0.6; range, 1.0–2.7). PET undetected lesions were small with $D_{max\ MR}$ ≤8 mm. Figure 2 shows the smallest PET detected lesion ($D_{max\ MR}$ = 7 mm) and 2 lesions undetected with PET ($D_{max\ MR}$ = 6 mm and 5 mm).

The results in the SRS group are presented in Table 2. Six lesions were identified in the SRS group of which 4/6 lesions were defined as "MRI positive" and suspected as metastatic tissue, whereas 2/6 lesions were defined as "MRI negative" and hence indicative of radiation necrosis (1 example shown in Fig. 3). All 6 lesions had ^{18}F-FACBC uptake (SUV_{max}: mean, 3.2 ± 1.1; range, 1.4–4.2; TBR: mean, 8.4 ± 3.2; range, 3.6–12.6) and were detected with PET ($D_{max\ MR}$ ≥15 mm). The 2 patients with "MRI-positive" lesions deceased 5 months after the PET/MRI examination. The 2 lesions defined as "MRI negative" were stable at the time of follow-up (10 and 7 months after PET/MRI), but 1 of the patients had 7 new brain lesions consistent with new metastasis.

PET parameters (SUV_{max}, TBR) for all lesions detected and not detected with PET are shown in Figure 4, demonstrating that all PET detected lesions had SUV_{max} ≥1.2 and TBR ≥3.6. Lesions from all included tumor origins showed ^{18}F-FACBC uptake, and the distributions of the PET parameters for the different tumor origins (lung cancer [n = 11], GI cancer [n = 8], malignant melanoma [n = 4], breast cancer [n = 1], thyroid cancer [n = 1]) are presented in Figure 5. No clear differences in SUV_{max} or TBR between the tumor origins were observed, but statistical tests of group differences were not performed due to small group sizes.

The MRI and PET tumor volumes for the PET detected lesions correlated significantly (r_s = 0.95, P < 0.001) and were not

FIGURE 1. Background VOI in normal brain parenchyma consisting of 6 consecutive crescent-shaped ROIs fused together, avoiding inclusion of ventricles and veins.

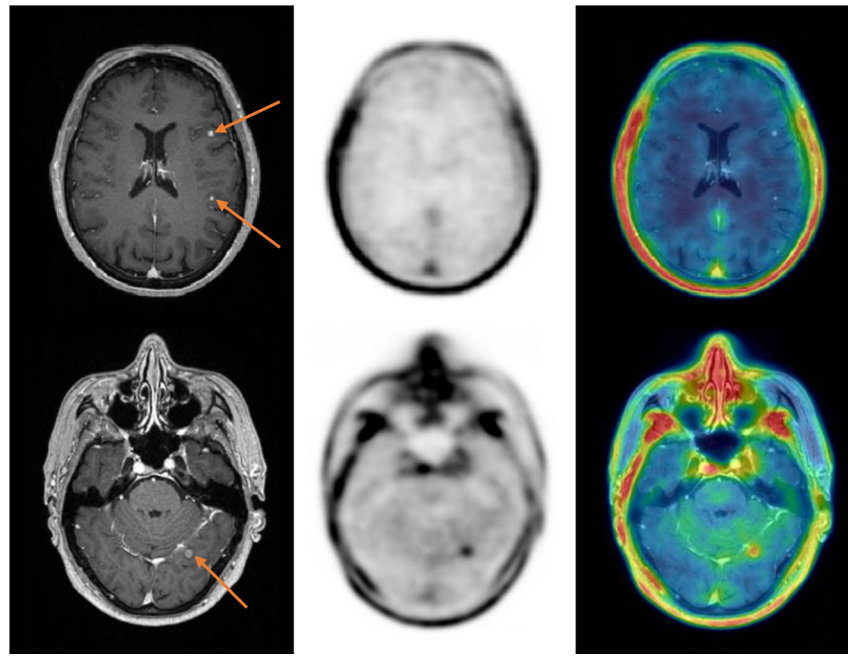

FIGURE 2. Upper row, Two "MRI-positive" lesions with $D_{max\ MR}$ of 6 mm and 5 mm (left, ce-MRI) not detected on PET (middle, ^{18}F-FACBC PET), shown on fused PET and MRI (right) (ID $13_{2,3}$; SUV scale from 0 to 1.6). Lower row, The smallest PET detected lesion with $D_{max\ MR}$ of 7 mm (ID 8_2; SUV scale from 0 to SUV_{max}).

significantly different ($P = 0.49$) (MRI: mean, 6.0 ± 7.8 mL; range, 0.1–27.0 mL; PET: mean, 6.9 ± 8.6 mL; range, 0.5–30.9 mL) (Fig. 6). The average spatial similarity of PET and MRI volumes measured by DSC was 0.66 ± 0.18 (range, 0.24–0.90). The lesion with lowest DSC is shown in Figure 7.

Dynamic PET

Time-activity curves for SUV_{max} and SUV_{mean} are shown in Figure 8. In the no-SRS group, 6/14 lesions had a TAC defined as plateau (slope II) and 8/14 lesions had a decreasing curve (slope III). In the SRS group, one lesion in a patient who deceased 5 months after PET/MRI scanning had a TAC curve defined as slope III, whereas the TAC curves of the other 5 lesions were defined as slope II. No lesion had an increasing curve (slope I). Both slope II and III were represented for lung cancer, GI cancer, and malignant melanoma, whereas the lesion originating from breast cancer had a slope III.

DISCUSSION

This study evaluated the use of ^{18}F-FACBC PET/MRI in 18 patients with brain metastases and is to our knowledge the largest study using ^{18}F-FACBC in this patient group. The majority of brain metastases demonstrated high uptake of ^{18}F-FACBC and low ^{18}F-FACBC uptake in normal brain tissue, resulting in generally high TBR. However, small brain metastases (<7 mm) were only detected by ce-MRI and not by ^{18}F-FACBC PET. Consequently, our findings demonstrated an inferior detection of brain metastases using ^{18}F-FACBC PET compared with ce-MRI.

The poor spatial resolution of PET imaging likely explains why ce-MRI performed better than ^{18}F-FACBC PET in the detection of small brain metastases. The limited spatial resolution cause reduced lesion uptake in small lesions (approximately 10 mm and smaller) in PET images due to partial volume effects, which limits the detectability.[38,39] Interestingly, a study by Bogsrud et al[23] reported

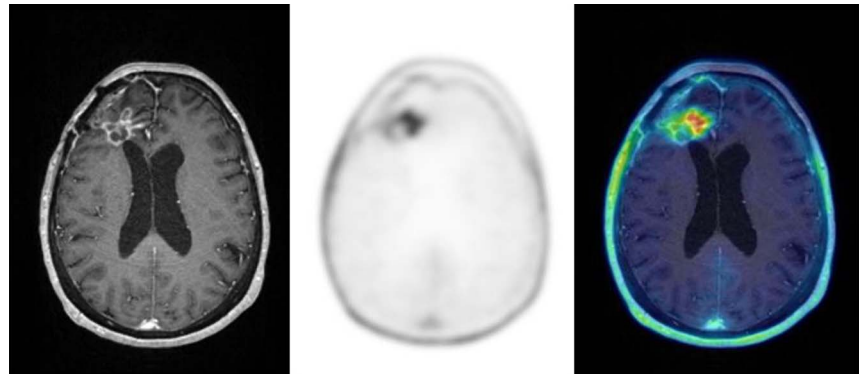

FIGURE 3. "MRI-negative" finding indicative of radiation necrosis on ce-MRI due to missing progression in a location with prior resection and SRS (ID 7, lung cancer) (left). ^{18}F-FACBC PET showed high uptake (middle) (SUV scale from 0 to SUV_{max}). Fused PET and ce-MRI (right).

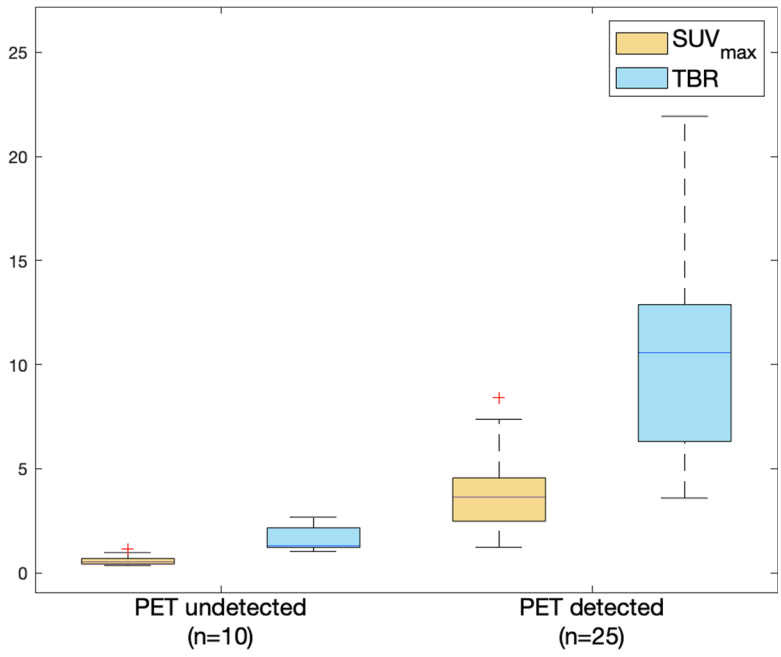

FIGURE 4. SUV_{max} and TBR for lesions detected and not detected with PET. Red markers (+) represent outliers.

detection of small satellite tumors of 2 to 4 mm in patients with suspected high-grade gliomas. All these tumors had high TBRs[4–18] that probably enabled detection below PET spatial resolution. The satellite tumors were undetectable on MRI, although this may be explained by the 5 to 14 days delay between MRI and PET/CT examinations. It can be noted that the PET/CT system (Biograph mCT) used in the study by Bogsrud et al[23] has shown a slightly improved detectability over the PET/MRI system (Biograph mMR) used in the current study, which may have further impacted the results.[37]

Brain metastases below 10 mm that were detected with ^{18}F-FACBC PET in our study had TBR approximately 4 to 5, whereas PET undetected metastases had TBR up to 2.7. Hence, for ^{18}F-FACBC PET detection of lesions with diameters below 10 mm, a TBR of approximately 4 may be required. The generally high TBR in the study by Bogsrud et al[23] (median, 21.6) may be due to the inclusion of high-grade gliomas, as TBR tends to increase with glioma tumor grade.[22,28] In studies using ^{11}C-MET and ^{18}F-FET in both gliomas and brain metastases, the average TBR was slightly

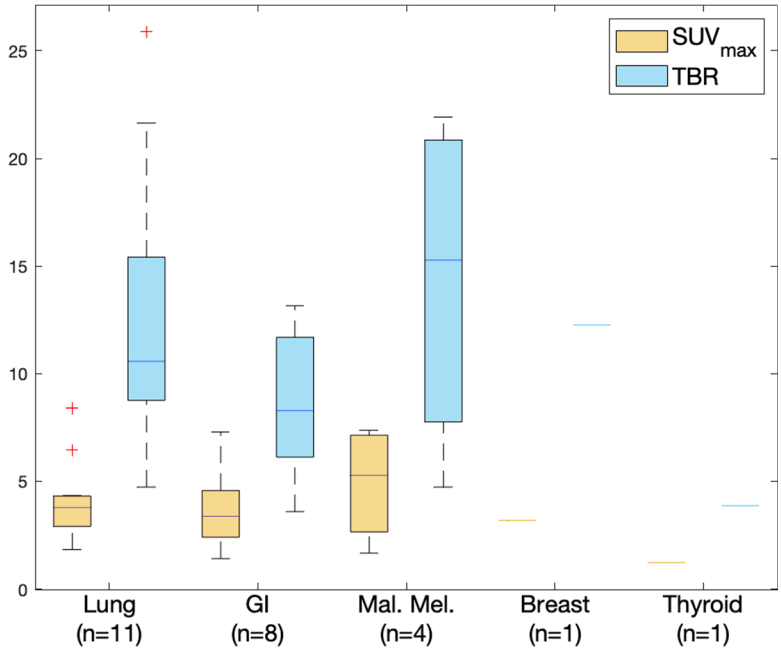

FIGURE 5. SUV_{max} and TBR for PET detected lesions of the different patient groups. Red markers (+) represent outliers.

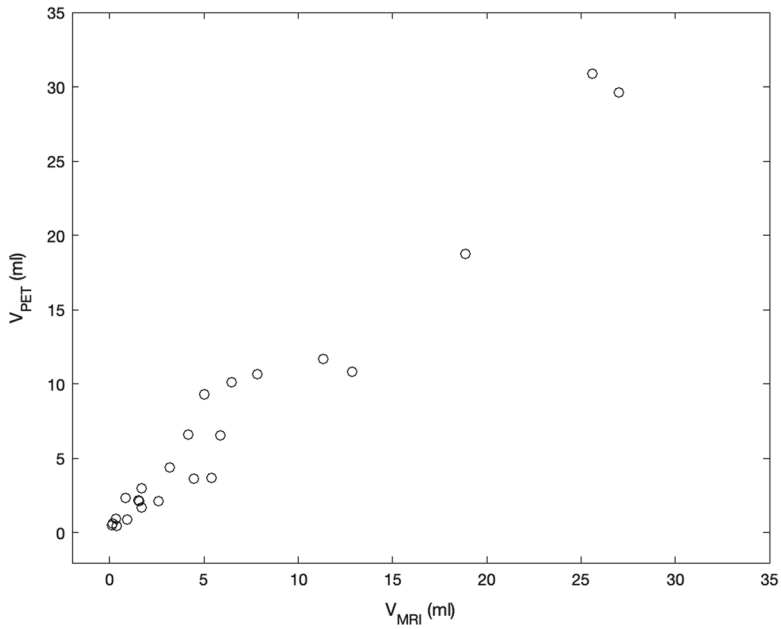

FIGURE 6. Volume of PET detected lesions defined in ce-MRI (V_{MRI}) versus ^{18}F-FACBC PET (V_{PET}). Significant correlation (r_s = 0.95, $P < 0.001$) between V_{MRI} and V_{PET}.

lower for brain metastases than for gliomas[40,41]; however, it is uncertain whether this difference is significant and whether it is unique for specific PET tracers. If brain metastases generally have lower AA uptake than gliomas, this may contribute to a reduced detectability for brain metastases.

Our findings suggest that ^{18}F-FACBC can produce significantly higher TBR for brain metastases (11.1 ± 6.0) than has been reported for ^{11}C-MET and ^{18}F-FET.[17–19,40,42–46] This potentially allows for detection of smaller brain metastases with ^{18}F-FACBC than for other AA PET tracers. However, brain metastases as small as 6 mm have been reported ^{18}F-FET positive in a study by Unterrainer et al.[44] They used a quantitative definition of ^{18}F-FET–positive metastases (TBR ≥ 1.6), whereas a visual definition was used in the current study as no such guideline exists for ^{18}F-FACBC. A visual definition is subjective, and a faint uptake could in some cases be observed, although not distinctly higher than surrounding tissue.

Although not all lesions were detected with PET, brain metastases from all the included primary cancers showed ^{18}F-FACBC uptake. No remarkable differences in ^{18}F-FACBC uptake were observed between the metastases of different tumor origins, but the groups were too small for statistical testing. The results are consistent with the ^{18}F-FET study by Unterrainer et al[44] where brain metastases originating from lung, breast, and melanoma did not show significantly different uptake. Larger groups are required to verify that brain metastases originating from different primary cancer show similar AA uptake.

In concordance with previous studies, ^{18}F-FACBC stands out among AA PET tracers by exhibiting uniquely low uptake in healthy brain tissue.[22,24,26–28,31,47] This difference is likely due to slight differences in the transport mechanisms by which the AA tracers cross the BBB. For accumulation in cancer cells, the primary mode of transport for ^{11}C-MET and ^{18}F-FET is the system L AA transport (LAT1) system.[20,48–51] Although ^{18}F-FACBC also uses LAT1, it has higher affinity to ASCT2 (alanine-serine-cysteine transporter 2).[51–53] A lack of and presence of ASCT2 expression on the luminal and abluminal side of BBB endothelial cells, respectively, may contribute to low ^{18}F-FACBC uptake by resulting in a low luminal uptake of ^{18}F-FACBC from blood and an increased abluminal ^{18}F-FACBC uptake from normal brain tissue. The low background uptake of ^{18}F-FACBC clearly allows for high tumor contrast.

MRI evaluations of brain tumors following radiation treatment present a clinical challenge, as MRI may not be able to distinguish malignant tissue from radiation necrosis as both show contrast enhancement.[54] Amino acid PET can potentially play an important

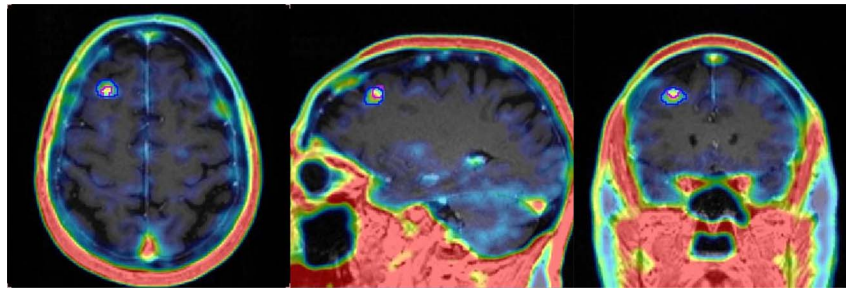

FIGURE 7. Fused PET/MRI scans of the lesion with the lowest spatial similarity between volumes defined on ^{18}F-FACBC (blue) and ce-MRI (cerise). The DSC for the volumes was 0.24 (SUV scale from 0 to SUV_{max}).

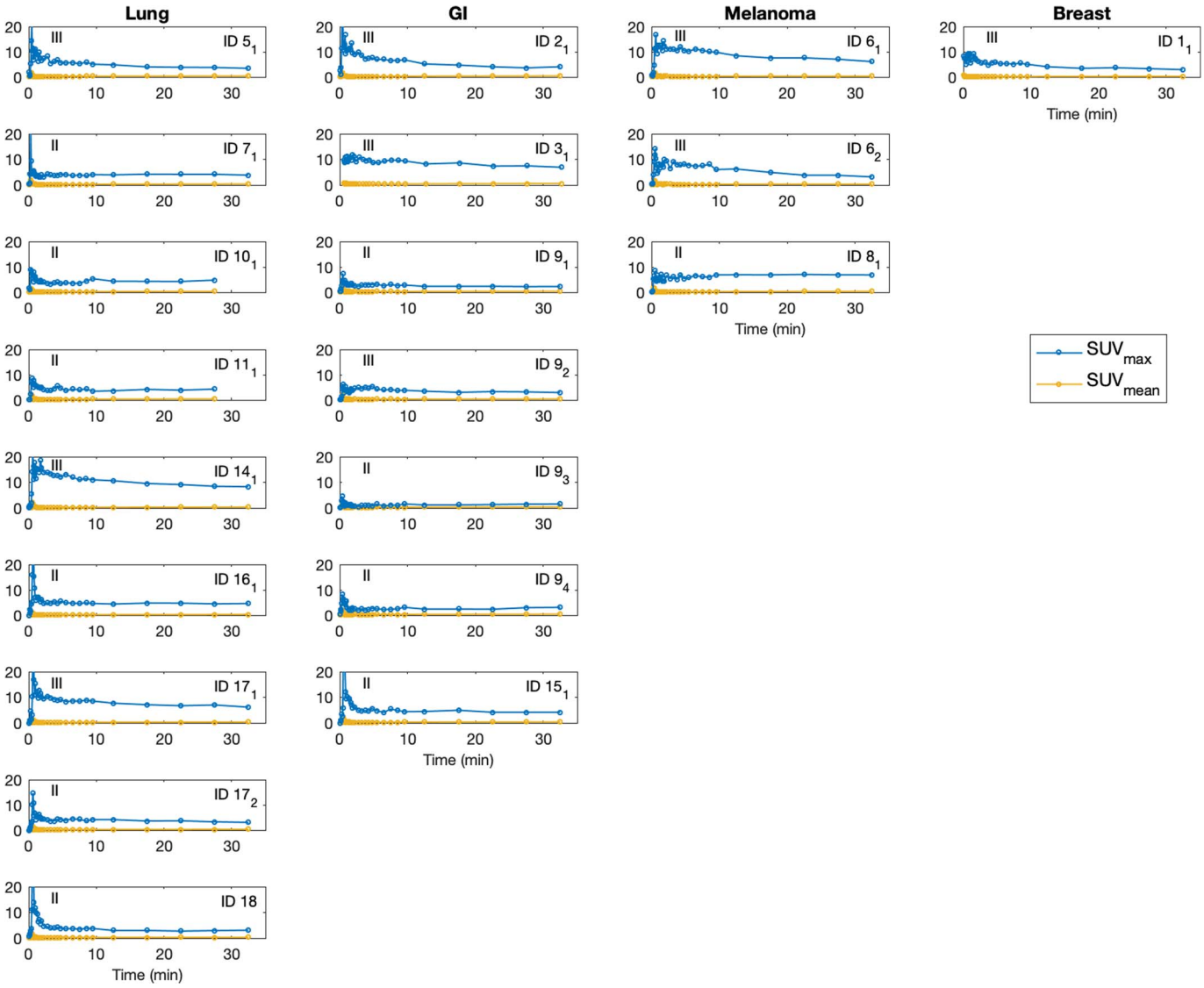

FIGURE 8. Time-activity curves for lesions (SUV_{max}) detected on PET with D_{max} MR >10 mm and normal brain tissue (SUV_{mean}). The slope characterization is denoted in each plot as Roman numerals and the patient ID with the lesion number as subscript.

role in this situation by providing metabolic information to better detect malignancies when MRI findings are equivocal. All 6 lesions in the SRS group had ^{18}F-FACBC uptake, but 2 lesions were suspected as radiation necrosis with MRI due to no progressive enlargement compared with MRI scans before PET/MRI. Follow-up MRI also showed that the 2 lesions remained stable, but one of the patients had 7 new brain lesions. Using follow-up MRI as reference might, however, be insufficient in patients treated with SRS as radiation necrosis may occur up to several years after radiation therapy and may also increase in size.[55,56] This exemplifies the diagnostic challenge in these patients, which is even more difficult as it is shown that radiation necrosis and viable metastatic tissue can coexist.[55] Thus, without histopathological verification and with the small cohort in the SRS group, our study yields inconclusive results regarding the value of ^{18}F-FACBC PET for differentiation between brain metastasis recurrence and radiation necrosis.

Recently, Parent et al[30] showed a significant difference in SUV_{max} of ^{18}F-FACBC PET between local brain metastasis recurrence and radiation necrosis in patients that had undergone SRS, verified by histopathology or follow-up MRI. They concluded that an SUV_{max} ≥1.3 differentiated recurrence from radiation necrosis, which points to recurrence for all the lesions in our SRS group. However, their study was limited by few samples (11 recurrent metastases and 4 radiation necrotic lesions). Furthermore, Parent et al did not report a significant difference in TBR between local recurrence and radiation necrosis, which was attributed to a variable tracer uptake in normal brain tissue. SUV_{max} in a 15-mm spherical background ROI was used as a reference, although SUV_{mean} in a crescent-shaped VOI could possibly have reduced the variability.[35] The patients in the no-SRS group in the current study will be followed after SRS treatment to further evaluate the accuracy of ^{18}F-FACBC in distinguishing viable tumor tissue from radiation necrosis. One can hypothesize that ^{18}F-FACBC PET could have a more important role in a follow-up setting than in the primary evaluation of brain metastases, but more studies using histopathology as reference should be performed to fully explore the tracer for this purpose.

Dynamic ^{18}F-FET PET has shown high diagnostic accuracy in differentiating brain metastasis recurrence from radiation necrosis

when combined with TBR.[17–19] Radiation necrosis has been associated with slowly increasing TAC curves, whereas recurrence show early peaks followed by a plateau or decreasing slope. ^{18}F-FACBC uptake in radiation necrosis has to our knowledge only been measured in the study by Parent et al,[30] showing a slight increase throughout the acquisition, although with a limited number of time points (5, 10, 30, 55 minutes). In the current study, all lesions showed early peaks followed by either a plateau or decreasing slope, also the lesions suspected as radiation necrosis with MRI. It is still unclear whether dynamic ^{18}F-FACBC PET analyses can be useful for distinguishing recurrent brain metastases from radiation necrosis.

The lack of guidelines for ^{18}F-FACBC PET volumetric analysis of brain tumors has resulted in inconsistent methods throughout the literature. This study used 41% of SUV_{max} to delineate tumor boundaries as this visually delineated the ^{18}F-FACBC uptake best for all lesion sizes. Previous ^{18}F-FACBC studies on brain metastases and gliomas have used 50% of SUV_{max}, thresholds based on uptake in reference tissue, and manual delineation.[22,25,31,47] In our study, no significant difference in tumor volume for ^{18}F-FACBC PET and ce-MRI was found; however, the spatial distribution was only partially similar. This spatial incongruence may indicate that ^{18}F-FACBC can detect tumor tissue beyond contrast enhancement on MRI, although the result may be affected by the delineation method. Similarly, Gempt et al[42] found that ^{18}F-FET PET and MRI volumes of brain metastases were not congruent, and that treatment planning based on only one of the modalities might cause undertreatment. It should, however, be noted that the mean time between MRI and PET examinations were 8 days (range, 3–33 days) in that study, which probably impacted the results. To generate guidelines for volumetric ^{18}F-FACBC PET analysis of brain tumors, further research comparing ^{18}F-FACBC PET with data from MRI, tumor resection, and/or image-localized biopsy needs to be conducted.

A strength of this study is the larger sample size of this patient group compared with earlier studies; however, the sample size is still limited, especially for evaluation of radiation necrosis in the SRS group. Differentiation of recurrence from radiation necrosis on MRI in the SRS group was based on increase in lesion size according to the RANO criteria.[34] However, this criterion can be discussed, and it has been shown in a study of more than 500 brain metastases that increase in lesion size after SRS was associated with longer survival compared with lesions exhibiting stable or decreased lesion size.[56] This indicates that lesion enlargement may represent reactive immune response instead of tumor regrowth, showing that increase in size is not necessarily a good indicator for recurrence. Thus, other features such as enlargement across anatomical boundaries, type of contrast enhancement, conspicuity of tumor margins, and complex evolution such as simultaneous regression and enlargement have been suggested indicative of radiation necrosis rather than tumor progression,[57,58] but this has not been considered in this study. Biopsy is the criterion standard for distinguishing tumor recurrence from radiation necrosis but was not included in this study because it is invasive and may cause complications. Another limitation is that one patient received immunotherapy the last month before PET/MRI. This can cause an increase in the size and number of metastases in the initial phase of the treatment related to the mechanisms of action of immunotherapy, which are later stabilized or regressed.[59] Furthermore, the study is limited by the patient heterogeneity, with regard to newly diagnosed and recurrent metastases as well as differences in tumor origins. The lack of standardization for volume delineation for ^{18}F-FACBC limits the validity of the volumetric results.

CONCLUSIONS

^{18}F-FACBC showed uptake in brain metastases originating from lung, GI, breast, and thyroid cancer, as well as malignant melanoma. The tracer is unique among AA PET tracers with a characteristic low uptake in healthy brain tissue resulting in a high tumor contrast. However, in small lesions, the ^{18}F-FACBC PET uptake was not sufficient for detection, and PET was inferior to MRI. ^{18}F-FACBC PET should be further evaluated in a follow-up setting for its opportunities to differentiate between tumor recurrence and radiation necrosis. Whether ^{18}F-FACBC PET can detect metastatic tumor tissue beyond ce-MRI should also be further explored.

ACKNOWLEDGMENTS

Special thanks to the bioengineers and radiographers at St. Olavs Hospital for patient preparations and image acquisitions, and to Katy-Olga Grøtte Stene for collecting patient information. We would also like to thank that Trond Mohn Foundation for supporting us with funding for the project.

REFERENCES

1. Nayak L, Lee EQ, Wen PY. Epidemiology of brain metastases. *Curr Oncol Rep*. 2012;14:48–54.
2. Ranjan T, Abrey LE. Current management of metastatic brain disease. *Neurotherapeutics*. 2009;6:598–603.
3. Klos KJ, O'Neill BP. Brain metastases. *Neurologist*. 2004;10:31–46.
4. Ostrom QT, Wright CH, Barnholtz-Sloan JS. Brain metastases: epidemiology. *Handb Clin Neurol*. 2018;149:27–42.
5. Park K, Bae GH, Kim WK, et al. Radiotherapy for brain metastasis and long-term survival. *Sci Rep*. 2021;11:8046.
6. Hall WA, Djalilian HR, Nussbaum ES, et al. Long-term survival with metastatic cancer to the brain. *Med Oncol*. 2000;17:279–286.
7. Achrol AS, Rennert RC, Anders C, et al. Brain metastases. *Nat Rev Dis Primers*. 2019;5:5.
8. Soliman H, Das S, Larson DA, et al. Stereotactic radiosurgery (SRS) in the modern management of patients with brain metastases. *Oncotarget*. 2016; 7:12318–12330.
9. Gaebe K, Li AY, Das S. Clinical biomarkers for early identification of patients with intracranial metastatic disease. *Cancers (Basel)*. 2021;13:5973.
10. Zakaria R, Das K, Bhojak M, et al. The role of magnetic resonance imaging in the management of brain metastases: diagnosis to prognosis. *Cancer Imaging*. 2014;14:8.
11. Galldiks N, Langen KJ, Albert NL, et al. PET imaging in patients with brain metastasis-report of the RANO/PET group. *Neuro Oncol*. 2019;21:585–595.
12. Kwee RM, Kwee TC. Dynamic susceptibility MR perfusion in diagnosing recurrent brain metastases after radiotherapy: a systematic review and meta-analysis. *J Magn Reson Imaging*. 2020;51:524–534.
13. Vander Borght T, Asenbaum S, Bartenstein P, et al. EANM procedure guidelines for brain tumour imaging using labelled amino acid analogues. *Eur J Nucl Med Mol Imaging*. 2006;33:1374–1380.
14. Langen K-J, Galldiks N, Hattingen E, et al. Advances in neuro-oncology imaging. *Nat Rev Neurol*. 2017;13:279–289.
15. Albert NL, Weller M, Suchorska B, et al. Response assessment in neuro-oncology working group and European Association for Neuro-Oncology recommendations for the clinical use of PET imaging in gliomas. *Neuro Oncol*. 2016;18:1199–1208.
16. Law I, Albert NL, Arbizu J, et al. Joint EANM/EANO/RANO practice guidelines/SNMMI procedure standards for imaging of gliomas using PET with radiolabelled amino acids and [^{18}F]FDG: version 1.0. *Eur J Nucl Med Mol Imaging*. 2019;46:540–557.
17. Galldiks N, Stoffels G, Filss CP, et al. Role of O-(2-(18)F-fluoroethyl)-L-tyrosine PET for differentiation of local recurrent brain metastasis from radiation necrosis. *J Nucl Med*. 2012;53:1367–1374.
18. Ceccon G, Lohmann P, Stoffels G, et al. Dynamic O-(2-^{18}F-fluoroethyl)-L-tyrosine positron emission tomography differentiates brain metastasis recurrence from radiation injury after radiotherapy. *Neuro Oncol*. 2017;19: 281–288.
19. Romagna A, Unterrainer M, Schmid-Tannwald C, et al. Suspected recurrence of brain metastases after focused high dose radiotherapy: can [(18)F] FET- PET overcome diagnostic uncertainties? *Radiat Oncol*. 2016;11:139.
20. Sun A, Liu X, Tang G. Carbon-11 and fluorine-18 labeled amino acid tracers for positron emission tomography imaging of tumors. *Front Chem*. 2017; 5:124.

21. Shoup TM, Olson J, Hoffman JM, et al. Synthesis and evaluation of [^{18}F]1-amino-3-fluorocyclobutane-1-carboxylic acid to image brain tumors. *J Nucl Med*. 1999;40:331–338.
22. Karlberg A, Berntsen EM, Johansen H, et al. ^{18}F-FACBC PET/MRI in diagnostic assessment and neurosurgery of gliomas. *Clin Nucl Med*. 2019;44:550–559.
23. Bogsrud TV, Londalen A, Brandal P, et al. ^{18}F-Fluciclovine PET/CT in suspected residual or recurrent high-grade glioma. *Clin Nucl Med*. 2019;44:605–611.
24. Kondo A, Ishii H, Aoki S, et al. Phase IIa clinical study of [^{18}F]fluciclovine: efficacy and safety of a new PET tracer for brain tumors. *Ann Nucl Med*. 2016;30:608–618.
25. Michaud L, Beattie BJ, Akhurst T, et al. ^{18}F-Fluciclovine (^{18}F-FACBC) PET imaging of recurrent brain tumors. *Eur J Nucl Med Mol Imaging*. 2020;47:1353–1367.
26. Tsuyuguchi N, Terakawa Y, Uda T, et al. Diagnosis of brain tumors using amino acid transport PET imaging with ^{18}F-fluciclovine: a comparative study with L-methyl-^{11}C-methionine PET imaging. *Asia Ocean J Nucl Med Biol*. 2017;5:85–94.
27. Wakabayashi T, Iuchi T, Tsuyuguchi N, et al. Diagnostic performance and safety of positron emission tomography using ^{18}F-fluciclovine in patients with clinically suspected high- or low-grade gliomas: a multicenter phase IIb trial. *Asia Ocean J Nucl Med Biol*. 2017;5:10–21.
28. Parent EE, Benayoun M, Ibeanu I, et al. [(18)F]Fluciclovine PET discrimination between high- and low-grade gliomas. *EJNMMI Res*. 2018;8:67.
29. Akhurst T, Beattie B, Gogiberidze G, et al. [^{18}F] FACBC imaging of recurrent gliomas: a comparison with [^{11}C] methionine and MRI. *J Nucl Med*. 2006;47(suppl 1):79P.
30. Parent EE, Patel D, Nye JA, et al. [(18)F]-Fluciclovine PET discrimination of recurrent intracranial metastatic disease from radiation necrosis. *EJNMMI Res*. 2020;10:148.
31. Johannessen K, Berntsen EM, Johansen H, et al. ^{18}F-FACBC PET/MRI in the evaluation of human brain metastases: a case report. *Eur J Hybrid Imaging*. 2021;5:7.
32. Sperduto PW, Kased N, Roberge D, et al. Summary report on the graded prognostic assessment: an accurate and facile diagnosis-specific tool to estimate survival for patients with brain metastases. *J Clin Oncol*. 2012;30:419–425.
33. Ladefoged CN, Hansen AE, Henriksen OM, et al. AI-driven attenuation correction for brain PET/MRI: clinical evaluation of a dementia cohort and importance of the training group size. *Neuroimage*. 2020;222:117221.
34. Lin NU, Lee EQ, Aoyama H, et al. Response assessment criteria for brain metastases: proposal from the RANO group. *Lancet Oncol*. 2015;16:e270–e278.
35. Unterrainer M, Vettermann F, Brendel M, et al. Towards standardization of (18)F-FET PET imaging: do we need a consistent method of background activity assessment? *EJNMMI Res*. 2017;7:48.
36. Dice LR. Measures of the amount of ecologic association between species. *Ecology*. 1945;26:297–302.
37. Øen SK, Aasheim LB, Eikenes L, et al. Image quality and detectability in Siemens biograph PET/MRI and PET/CT systems—a phantom study. *EJNMMI Phys*. 2019;6:16.
38. Soret M, Bacharach SL, Buvat I. Partial-volume effect in PET tumor imaging. *J Nucl Med*. 2007;48:932–945.
39. Karlberg AM, Saether O, Eikenes L, et al. Quantitative comparison of PET performance-Siemens biograph mCT and mMR. *EJNMMI Phys*. 2016;3:5.
40. Grosu AL, Astner ST, Riedel E, et al. An interindividual comparison of *O*-(2-[^{18}F]fluoroethyl)-L-tyrosine (FET)- and L-[methyl-^{11}C]methionine (MET)-PET in patients with brain gliomas and metastases. *Int J Radiat Oncol Biol Phys*. 2011;81:1049–1058.
41. Terakawa Y, Tsuyuguchi N, Iwai Y, et al. Diagnostic accuracy of ^{11}C-methionine PET for differentiation of recurrent brain tumors from radiation necrosis after radiotherapy. *J Nucl Med*. 2008;49:694–699.
42. Gempt J, Bette S, Buchmann N, et al. Volumetric analysis of F-18-FET-PET imaging for brain metastases. *World Neurosurg*. 2015;84:1790–1797.
43. Tsuyuguchi N, Sunada I, Iwai Y, et al. Methionine positron emission tomography of recurrent metastatic brain tumor and radiation necrosis after stereotactic radiosurgery: is a differential diagnosis possible? *J Neurosurg*. 2003;98:1056–1064.
44. Unterrainer M, Galldiks N, Suchorska B, et al. ^{18}F-FET PET uptake characteristics in patients with newly diagnosed and untreated brain metastasis. *J Nucl Med*. 2017;58:584–589.
45. Yomo S, Oguchi K. Prospective study of (11)C-methionine PET for distinguishing between recurrent brain metastases and radiation necrosis: limitations of diagnostic accuracy and long-term results of salvage treatment. *BMC Cancer*. 2017;17:713.
46. Minamimoto R, Saginoya T, Kondo C, et al. Differentiation of brain tumor recurrence from post-radiotherapy necrosis with ^{11}C-methionine PET: visual assessment versus quantitative assessment. *PLoS One*. 2015;10:e0132515.
47. Karlberg A, Berntsen EM, Johansen H, et al. Multimodal (18)F-Fluciclovine PET/MRI and ultrasound-guided neurosurgery of an anaplastic oligodendroglioma. *World Neurosurg*. 2017;108:989.e1–989.e8.
48. Habermeier A, Graf J, Sandhöfer BF, et al. System L amino acid transporter LAT1 accumulates *O*-(2-fluoroethyl)-L-tyrosine (FET). *Amino Acids*. 2015;47:335–344.
49. Heiss P, Mayer S, Herz M, et al. Investigation of transport mechanism and uptake kinetics of *O*-(2-[^{18}F] fluoroethyl)-L-tyrosine in vitro and in vivo. *J Nucl Med*. 1999;40:1367–1373.
50. Okubo S, Zhen HN, Kawai N, et al. Correlation of L-methyl-^{11}C-methionine (MET) uptake with L-type amino acid transporter 1 in human gliomas. *J Neurooncol*. 2010;99:217–225.
51. Ono M, Oka S, Okudaira H, et al. Comparative evaluation of transport mechanisms of trans-1-amino-3-[^{18}F]fluorocyclobutanecarboxylic acid and L-[methyl-^{11}C]methionine in human glioma cell lines. *Brain Res*. 2013;1535:24–37.
52. Okudaira H, Nakanishi T, Oka S, et al. Corrigendum to "kinetic analyses of trans-1-amino-3-[^{18}F]fluorocyclobutanecarboxylic acid transport in *Xenopus laevis* oocytes expressing human ASCT2 and SNAT2" (Nucl. Med. Biol. 2013;40:670–675). *Nucl Med Biol*. 2015;42:513–514.
53. Pickel TC, Voll RJ, Yu W, et al. Synthesis, radiolabeling, and biological evaluation of the cis stereoisomers of 1-amino-3-fluoro-4-(fluoro-(18)F) Cyclopentane-1-carboxylic acid as PET imaging agents. *J Med Chem*. 2020;63:12008–12022.
54. Brandsma D, van den Bent MJ. Pseudoprogression and pseudoresponse in the treatment of gliomas. *Curr Opin Neurol*. 2009;22:633–638.
55. Shah R, Vattoth S, Jacob R, et al. Radiation necrosis in the brain: imaging features and differentiation from tumor recurrence. *Radiographics*. 2012;32:1343–1359.
56. Patel TR, McHugh BJ, Bi WL, et al. A comprehensive review of MR imaging changes following radiosurgery to 500 brain metastases. *AJNR Am J Neuroradiol*. 2011;32:1885–1892.
57. Lasocki A, Sia J, Stuckey SL. Improving the diagnosis of radiation necrosis after stereotactic radiosurgery to intracranial metastases with conventional MRI features: a case series. *Cancer Imaging*. 2022;22:33.
58. Nichelli L, Casagranda S. Current emerging MRI tools for radionecrosis and pseudoprogression diagnosis. *Curr Opin Oncol*. 2021;33:597–607.
59. Wolchok JD, Hoos A, O'Day S, et al. Guidelines for the evaluation of immune therapy activity in solid tumors: immune-related response criteria. *Clin Cancer Res*. 2009;15:7412–7420.